Direct evidence of dopant segregation in Gd-doped ceria

Zhi-Peng Li, Toshiyuki Mori, Graeme John Auchterlonie, Jin Zou, and John Drennan

---

Articles you may be interested in

Formation of the dopant-oxygen vacancy complexes and its influence on the photoluminescence emissions in Gd-doped HfO2
J. Appl. Phys. **116**, 123505 (2014); 10.1063/1.4896371

Ordered structures of defect clusters in gadolinium-doped ceria
J. Chem. Phys. **134**, 224708 (2011); 10.1063/1.3599089

Oxygen surface exchange studies in thin film Gd-doped ceria
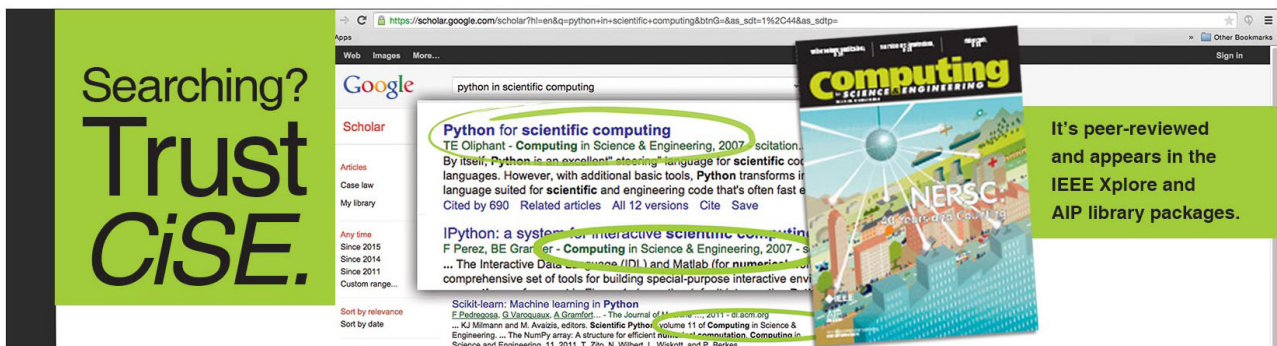Appl. Phys. Lett. **92**, 243109 (2008); 10.1063/1.2938028

Tunable electrical conductivity in nanoscale Gd-doped ceria thin films
Appl. Phys. Lett. **90**, 263108 (2007); 10.1063/1.2752028

Strain relaxation by directionally aligned precipitate nanoparticles in the growth of single-crystalline Gd-doped ceria thin films
Appl. Phys. Lett. **84**, 708 (2004); 10.1063/1.1644035

Direct evidence of dopant segregation in Gd-doped ceria

Zhi-Peng Li,[1,a)] Toshiyuki Mori,[1] Graeme John Auchterlonie,[2] Jin Zou,[2,3] and John Drennan[2]

[1]*Global Research Center for Environment and Energy Based on Nanomaterials Science, National Institute for Materials Science, Tsukuba, Ibaraki 305-0044, Japan*
[2]*Centre for Microscopy and Microanalysis, The University of Queensland, St. Lucia, Brisbane, Queensland 4072, Australia*
[3]*School of Engineering, The University of Queensland, St. Lucia, Brisbane, Queensland 4072, Australia*

Microstructures and segregations of dopants and associated oxygen vacancies in gadolinium-doped ceria (GDC) have been characterized by high-resolution transmission electron microscopy (HRTEM) and scanning TEM (STEM). Diffuse scattering was detected in 25 at. % GDC (25GDC) in comparison to 10GDC, which is ascribed to nanodomain formation in 25GDC. HRTEM, dark-field, and STEM Z-contrast imaging investigations all provide direct evidence for dopant segregation in doped ceria. It is illustrated that dopant cations cannot only segregate in grain interior forming larger nanodomains but also at grain boundary forming smaller ones. Detailed analyses about nanodomain formation and related dopant segregation behaviors are then elucidated. © *2011 American Institute of Physics*. [doi:10.1063/1.3556650]

Approaching to higher ionic conductivity is critical for intermediate temperature solid oxide fuel cells (IT-SOFCs) and has been actively sought for many years.[1,2] Rare-earth doped ceria has emerged as one promising alternative to conventional yttria-stabilized zirconia for IT-SOFCs due to its relatively high conductivity.[3] Nevertheless, ionic conductivity is sensitive to dopant type and concentration. The ionic conductivity will go through a maximum at a certain doping level (10–20 at. %) but then decrease even though it is far below dopant solubility.[3,4] One possible reason is the clustering of defects,[4] and another is grain boundary resistance originated from the space charge layer.[5] It is also reported that lattice distortion in heavily doped ceria can be ascribed to conductivity decrease.[6] Recently, investigations elucidated that nanodomains widely observed in rare-earth (Y,[7] La,[8] Sm,[9,10] Gd,[9,11] Tb,[12] Dy,[10,13] Ho,[14] and Yb[9,10]) doped ceria, could be responsible for the conductivity decrease. The nanodomains, with local ordered structures, can reduce the mobility of oxygen vacancies, leading to a decrease in ionic conductivity. Similarly, dopant segregation in nanodomains is also anticipated. Even though dopant segregation have been theoretically deduced decades ago,[15] direct experimental approaches to clarify such behaviors are hampered by relatively low doping concentration and analytical sensitivity of the techniques employed. Moreover, such nanodomains were only observed at grain interior, and investigations of spatial distributions of dopants at intergranular region, are still insufficient. Since the distribution and segregation of dopants has strong influences on microstructures and other properties of materials,[16] it is essential to obtain detailed understanding of such behaviors in order to develop high quality electrolytes and ionic conductors.

To seek direct evidence of dopant segregation in doped ceria, we made use of a combination of various techniques, namely, high-resolution transmission electron

microscopy (HRTEM), selected-area electron diffraction (SAED), electron energy loss spectroscopy (EELS), dark-field (DF) imaging and high-angle annular DF (HAADF) imaging operated in scanning TEM (STEM) mode. Gadolinium-doped ceria (GDC) was selected as the mode system because of its highest ionic conductivity among doped ceria electrolytes.[2,4] GDC nanopowders were synthesized by ammonium carbonate coprecipitation method.[8] Calcined nanopowders were isostatically pressed into cylindrical pellet and the compact green body was sintered at 1400 °C for 6 h to produce dense ceramic tablet. Microstructural features were characterized by a HRTEM (JEOL JEM-2000EX) and a STEM (FEI, Tecnai F20) equipped with a HAADF detector. Owing to different scattered angles of different elements, HAADF imaging is effective for local characterization of heterogeneities and spatial distributions of various constituents by being directly related to chemical contrast in the images.

Figure 1 compares GDC samples with different dopant concentrations. SAED patterns clearly demonstrate that as dopant concentration increases from 10 to 25 at. %, diffuse scatterings begin to appear. Their appearance indicates that the short-range ordered structure occurs in 25GDC. Furthermore, EELS investigation of oxygen K edge reveals a significant enhancement of B peak in 25GDC [Fig. 1(i)]. Such a fine structure evolution in EELS spectrum can be interpreted as a result of the enhancement of local oxygen vacancy
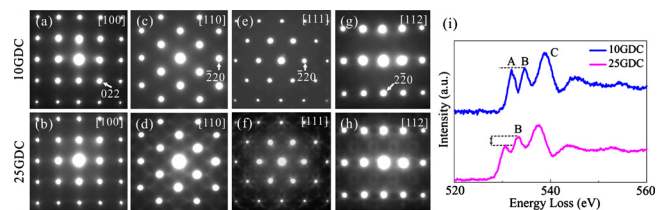

FIG. 1. (Color online) SAED patterns of 10GDC [(a), (c), (e), and (g)] and 25GDC [(b), (d), (f), and (h)] observed from different ZA; (i) is the comparison of EELS results of oxygen adsorption K edge of 10GDC and 25GDC, respectively.

a)Author to whom correspondence should be addressed. Tel.: +81-29-8513354 Extn. 8544. FAX: +81-29-8604712. Electronic mail: li.zhipeng@nims.go.jp.
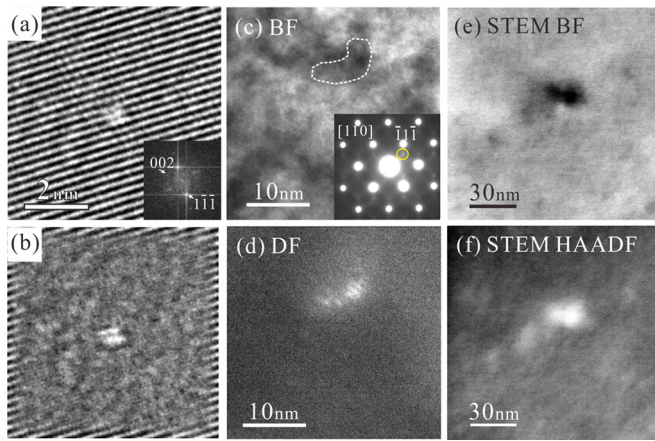
FIG. 2. (Color online) (a) HRTEM image of one grain interior in 25GDC, inset is the corresponding diffractogram; (b) is the related IFFT result of (a) by excluding diffraction spots originating from fluorite ceria. (c) HRTEM image of nanodomain observed at grain interior in 25GDC, inset is the related SAED pattern; (d) is the corresponding DF image; (e) STEM BF image of nanodomain observed at grain interior in 25GDC; (f) is the corresponding HAADF image.
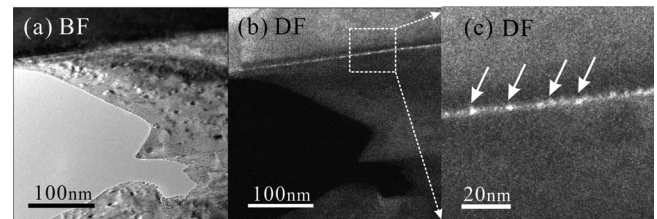

FIG. 3. (a) BF TEM image of one typical intergranular region observed in 25GDC; (b) is the corresponding DF image revealing that the grain boundary with bright contrast is ascribed to the diffuse scattering in SAED pattern; (c) is the zoomed in region denoted by dashed square in (b), clearly demonstrating the dopant segregation at grain boundary.

ordering.[17] These results indirectly suggest that nanodomain formation is associated with enhanced ordering of oxygen vacancies, which is consistent with previous reports.[9,10] Also, it is expected that dopant cations will aggregate and segregate in doped ceria and lead to nanodomain formation. In order to address this issue, further investigations of dopant distribution and segregation behaviors in heavily doped ceria are needed and thus have been conducted afterwards.

Figure 2(a) is a bright-field (BF) HRTEM image of 25GDC and the corresponding diffractogram is inserted. A slight lattice distortion accompanied with brighter contrast in the ceria lattice can be clearly seen. Extrapolating the diffractogram by filtering matrix information, only a specific region is retained in the related inverse fast Fourier transform (IFFT) image [Fig. 2(b)]. It is demonstrated that such region is different from its neighboring ceria as the origin of newly appeared diffraction features in the diffractogram. Due to the inhomogeneity of doped ceria, this region can be recognized as a nanodomain arising from the segregation of dopants as aforementioned. Figure 2(c) represents another nanodomain, denoted by a dashed line and embedded in a fine-grained ceria while with slightly distorted microstructure to that of adjacent matrix. However, since HRTEM is the phase-contrast imaging, the contrast cannot be necessarily intuitively interpreted. Therefore, other techniques, especially those with chemical analysis, should be employed. From corresponding SAED pattern [the inset in Fig. 2(c)], the diffused scattering feature near the central electron beam (highlighted by the circle) was selected to perform DF imaging. Related DF image [Fig. 2(d)] shows that the nanodomain exhibits bright contrast while nearby region is dark. Therefore, it provides strong evidence that the appearance of diffuse scatterings that has been widely observed in rare-earth doped ceria should be ascribed to nanodomain formation. Figure 2(e) is the STEM BF image of one grain interior in 25GDC. The strong intensity difference between the nanosized region and matrix indicates the formation of a nanodomain. To verify such assumption, STEM HAADF imaging is conducted in the same area and the related HAADF image is represented in Fig. 2(f). Note that the strong intensity only appears at the

same region as in Fig. 2(e), while with inverse contrast. Due to its chemical sensitivity to constituent elements of HAADF imaging, it indicates that such a bright region in Fig. 2(f) should be attributed to the presence of elements with higher atomic number (high-Z) than those in the dark region. In this case, Gd (Z=64) is the only heavier element than host cerium (Z=58) in the 25GDC sample. It is thus easier to distinguish lattice sites with the assembly of Gd or Ce cations. Additionally, the intensity contrast difference only occurs in the nanosized region while neighboring ceria is homogeneous with even contrast, which excludes the possibility of contrast modulation induced by height difference in such a small area. Therefore, Fig. 2(f) illustrates the enrichment of Gd at nanodomain region and supports previous hypothesis that nanodomain was formed due to the aggregation and segregation of dopants.[8–14]

Since plenty of grain boundaries are presented in polycrystalline ceramics, it is reasonable to assume that these boundaries also have strong effect on dopant distribution and segregation behaviors. This is because that grain boundary is usually considered as the defect center in polycrystalline materials and has larger volume than grain interior as the accommodation of extra atoms, ions, impurities, or defects.[16] Even though dopant segregation at grain boundary in GDC has been assumed or expected to exist in previous studies,[18,19] direct evidence is still deficient. Therefore, dopant segregation at grain boundaries has also been sought in this work. Figure 3(a) is a typical TEM BF image showing the intergranular region in 25GDC. The target grain was tilted along [110] ZA to ensure the grain boundary plane was approximately parallel to the incident electron beam. The diffuse scattering in SAED pattern was selected for DF imaging, and the corresponding DF image is shown in Fig. 3(b) with bright contrast in grain boundary in comparison to vicinal grain interiors with dark contrast. This implies that the grain boundary with enhanced brightness is enriched in constituents different from those in vicinal grain interiors. Figure 3(c) is a magnified region at the grain boundary denoted by a dashed square in Fig. 3(b). Note that separated nanodomain with brighter contrast, denoted by arrows in Fig. 3(c), occur at the highlighted grain boundary. These bright nanodomains can be easily discerned at grain boundaries in DF image, indicating a difference in microstructures or compositions between them and neighboring grain interiors. It is believed that formation of such nanodomains is accounted by dopant adsorption and segregation at the grain boundary. This accessible since it has been widely acknowledged that grain boundaries can act as infinite sources and sinks for atoms or vacancies[15] and most dopants or impurities can thus be
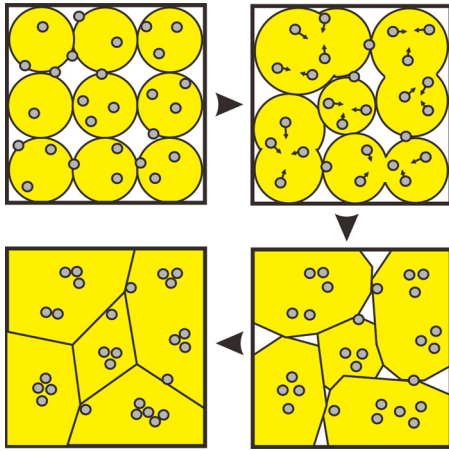
FIG. 4. (Color online) Schematic diagram illustrates the morphology discrepancy of dopant segregation at grain interiors and grain boundaries, associated with the grain growth during sintering process.

trapped to accommodate at grain boundaries or multiple grain junctions where more adsorption sites can be provided.[20] Analogous phenomenon, the Gd enrichment at grain boundary in 25GDC, has been verified by laser-assisted three-dimensional atom probe recently.[21] Our recent detections also illustrate that rare-earth elements can diffuse and segregate at grain boundaries.[22] Similar observation that rare-earth element (La) is preferentially segregated at grain boundary has also been demonstrated in La/Si_3N_4 ceramics.[23] However, such dopant segregation at grain boundary is quite different from the solute segregation to grain boundaries reported in MgO-doped Al_2O_3 and Y-doped TiO_2.[24] Although detailed mechanism is unclear here, it is reasonable to assume that the dopant-defect interaction is the driving force for dopant segregation rather than the solute segregation at grain boundary. Besides nanodomain formation in grain interior, it reveals that grain boundary segregation can contribute to the appearance of diffuse scattering features in SAED patterns as well.

Note the discrepancy of nanodomain morphology; the size of nanodomains detected in grain interiors is much larger than that at grain boundaries. This can be rationalized by taking into account the sintering process as follows. Initially, dopants randomly distribute in polycrystalline ceria [Fig. 4(a)]. The high temperature sintering proceeding will consequently enhance the mobility and interactions of dopants and associated oxygen vacancies. This will lead to aggregation of all heterogeneities in the ceria matrix [Fig. 4(b)]. On the other hand, grain growth will also occur [Fig. 4(b)]. Nearby contact grains will grow and coalescence will simultaneously take place, at the expense of related grain boundaries. This will further enhance the diffusivity, aggregation, and segregation of dopants and associated oxygen vacancies, arising from the decrease in block/trap effects caused by gain boundaries. Particularly, when some grain boundaries disappear, it can also be interpreted that the initial aggregation/segregation of dopants or oxygen vacancies at the grain boundaries actually occurs at the newly appeared grain interiors [Fig. 4(c)]. This can illustrate the final morphology that larger nanodomains widely exist in grain inte-

riors while those of much smaller size are located at grain boundaries [Fig. 4(d)].

To summarize, nanodomain formation, associated with oxygen vacancy ordering and dopant segregation, has been characterized by comprehensive TEM techniques, including high resolution imaging, SAED, EELS, DF, and HAADF imaging. SAED studies demonstrate the formation of short-range ordered structures as dopant concentration increases, which is attributed to nanodomains formation, accompanied with enhanced oxygen vacancy ordering verified by EELS analyses. Based on HRTEM, DF, and STEM HAADF imaging investigations, this study provides unambiguous verification of nanodomain formation at grain interior associated with dopant segregation. Furthermore, it also reveals that dopant cations not only segregate at grain interior in bigger size but also at grain boundaries in smaller size. We strongly believe that these investigations will significantly assist a comprehensive understanding of dopant distribution and segregation behaviors in rare-earth doped ceria, related microstructures evolution and the development of ceramic materials in SOFCs applications.

[1]S. Kartha and P. Grimes, Phys. Today **47**(11), 54 (1994).
[2]B. C. H. Steele and A. Heinzel, Nature (London) **414**, 345 (2001).
[3]S. M. Haile, Acta Mater. **51**, 5981 (2003).
[4]H. Inaba and H. Tagawa, Solid State Ionics **83**, 1 (1996).
[5]X. Guo and R. Waser, Solid State Ionics **173**, 63 (2004).
[6]G. B. Balazs and R. S. Glass, Solid State Ionics **76**, 155 (1995).
[7]T. Mori, J. Drennan, Y. Wang, G. Auchterlonie, J. G. Li, and A. Yago, Sci. Technol. Adv. Mater. **4**, 213 (2003).
[8]T. Mori, J. Drennan, Y. Wang, J. H. Lee, J. G. Li, and T. Ikegami, J. Electrochem. Soc. **150**, A665 (2003).
[9]D. R. Ou, T. Mori, F. Ye, T. Kobayashi, J. Zou, G. Auchterlonie, and J. Drennan, Appl. Phys. Lett. **89**, 171911 (2006).
[10]D. R. Ou, T. Mori, F. Ye, J. Zou, G. Auchterlonie, and J. Drennan, Phys. Rev. B **77**, 024108 (2008).
[11]Z. P. Li, T. Mori, F. Ye, D. R. Ou, J. Zou, and J. Drennan, Microsc. Microanal. **17**, 49 (2011).
[12]F. Ye, T. Mori, D. R. Ou, J. Zou, G. Auchterlonie, and J. Drennan, J. Appl. Phys. **101**, 113528 (2007).
[13]T. Mori, T. Kobayashi, Y. Wang, J. Drennan, T. Nishimura, J. G. Li, and H. Kobayashi, J. Am. Ceram. Soc. **88**, 1981 (2005).
[14]D. R. Ou, T. Mori, F. Ye, J. Zou, G. Auchterlonie, and J. Drennan, J. Electrochem. Soc. **154**, B616 (2007).
[15]M. F. Yan, R. M. Cannon, and H. K. Bowen, J. Appl. Phys. **54**, 764 (1983).
[16]M. P. Seah, J. Phys. F: Met. Phys. **10**, 1043 (1980).
[17]J. Yuan, T. Hirayama, Y. Ikuhara, and T. Sakuma, Micron **30**, 141 (1999).
[18]Z. Zhang, W. Sigle, M. Ruhle, E. Jud, and L. J. Gauckler, Acta Mater. **55**, 2907 (2007).
[19]Y. Lei, Y. Ito, and N. D. Browning, J. Am. Ceram. Soc. **85**, 2359 (2002).
[20]C. M. Wang, G. S. Cargill, H. M. Chan, and M. P. Harmer, Acta Mater. **48**, 2579 (2000).
[21]F. Li, T. Ohkubo, Y. M. Chen, M. Kodzuka, F. Ye, D. R. Ou, T. Mori, and K. Hono, Scr. Mater. **63**, 332 (2010).
[22]Z. P. Li, T. Mori, G. Auchterlonie, J. Zou, and J. Drennan (unpublished).
[23]N. Shibata, S. J. Pennycook, T. R. Gosnell, G. S. Painter, W. A. Shelton, and P. F. Becher, Nature (London) **428**, 730 (2004).
[24]K. K. Soni, A. M. Thompson, M. P. Harmer, D. B. Williams, J. M. Chabala, and R. L. Setti, Appl. Phys. Lett. **66**, 2795 (1995).